Open Forum Infectious Diseases

MAJOR ARTICLE

Differential Gene Expression Profiling in Alveolar Echinococcosis Identifies Potential Biomarkers Associated With Angiogenesis

Maiweilidan Yimingjiang,[1] Abudusalamu Aini,[2] Talaiti Tuergan,[3] and Wei Zhang[1]

[1]Department of Pathology, The First Affiliated Hospital of Xinjiang Medical University, Xinjiang, China, [2]Hepatopancreatobiliary Center, Beijing Tsinghua Changgung Hospital, School of Clinical Medicine, Tsinghua University, Beijing, China, and [3]Department of Hepatic Hydatid and Hepatobiliary Surgery, Digestive and Vascular Surgery Center, The First Affiliated Hospital of Xinjiang Medical University, Xinjiang, China

Background. Alveolar echinococcosis (AE) is a worldwide zoonosis caused by *Echinococcus multilocularis*. Alveolar echinococcosis is a severe chronic parasitic disease that exhibits a tumor-like growth, with the potential for invasion and distant metastasis; however, the molecular mechanism underlying this condition remains unclear.

Methods. Transcriptome analyses were performed to detect differentially expressed genes (DEGs) in samples from patients with AE with invasion and distant metastasis. The results were further verified by immunohistochemistry.

Results. A total of 1796 DEGs were identified, including 1742 upregulated and 54 downregulated DEGs. A subsequent functional analysis showed that the significant DEGs were involved in the angiogenesis process. Immunohistochemical analysis confirmed the reliability of the transcriptomic data.

Conclusions. These results suggest that angiogenesis is a possible mechanism underlying the tumor-like biological behavior observed during *E multilocularis* infection. Genes related to this process may play important roles in AE invasion and distant metastasis.

Keywords. alveolar echinococcosis; angiogenesis; invasion; transcriptome.

Echinococcosis represents a major public health issue in many countries and is prevalent in the northern hemisphere. The disease can be transmitted between carnivores (definitive host) and a large number of mammalian species, including humans, as accidental intermediate hosts; therefore, this condition is associated with great socioeconomic consequences and a high disease burden in endemic areas [1, 2]. The treatment and control of echinococcosis depend mainly on surgical operation and chemotherapy using benzimidazoles [3–5]. Cystic echinococcosis (CE) and alveolar echinococcosis (AE) are the 2 major forms of the disease in humans. Alveolar echinococcosis is a life-threatening chronic parasitic infection caused by the metacestode larval stages of the fox tapeworm *Echinococcus multilocularis* that is characterized by intense granulomatous infiltration around the parasite and results in a multivesicular parasitic tissue that grows infiltratively, similar to a malignant tumor, into the surrounding host tissue [6]. *Echinococcus multilocularis* larvae primarily affect the liver, accompanied by local invasion and distant metastasis to different organs, such as the lungs, brain, and kidneys, during prolonged infection; the lesions involve important blood vessels and bile ducts in most cases, thus hampering or precluding radical resection [7–9]. Although many studies have examined the mechanisms of initial infection and disease progression, very little is known about the molecular basis of the tumor-like biological behavior of AE.

Angiogenesis is recognized as the growth and remodeling process via which an initial vascular system is modified to form functional blood vessels [10]. This is accomplished by several anti- and proangiogenic factors that coordinate the functions of endothelial and smooth muscle cells [11]. Among them, members of the vascular endothelial growth factor (VEGF) and angiopoietin (Ang) families play a predominant role in regulating the migration, survival, and proliferation of endothelial cells (ECs) [12–14]. Angiogenesis plays an essential role in the process of tissue growth and regeneration and wound healing. However, pathological angiogenesis caused by the imbalance of these factors is a hallmark of cancer [15] and is related to many pathological conditions, including parasitic infection [16]. The nutrient supply and metabolite excretion, which are indispensable for the growth, maturation, and

Received 05 September 2022; editorial decision 17 January 2023; accepted 26 January 2023; published online 31 January 2023

Correspondence: Dr. Wei Zhang, Department of Pathology, The First Affiliated Hospital of Xinjiang Medical University, 137 Liyushan Southern Road, Urumqi, Xinjiang 830054, China (zwyhr100@163.com).

Open Forum Infectious Diseases®

https://doi.org/10.1093/ofid/ofad031

invasion of parasites in a host, depend on the circulatory system. Neovascularization during a parasitic infection can be activated by various factors produced by the parasites themselves, such as glucose phosphate isomerase [17]. Myeloid-derived suppressor cells are also activated and enriched during parasitic infections [18] and have been reported to secrete angiogenic factors, such as VEGF, to promote host angiogenesis during CE infection [19, 20]. During *E multilocularis* infection, an apparent neovascularization occurs in the AE lesion, particularly at the host-parasite interface, as described previously [21]. However, the molecular mechanism underlying the relationship between angiogenesis and invasion and distant metastasis during the process of *E multilocularis* infection remains unclear.

In the present study, to elucidate the molecular mechanism underling the invasion and distant metastasis observed during *E multilocularis* infection, transcriptome analyses were performed using high-throughput ribonucleic acid (RNA) sequencing, to detect the DEGs in the tissue of patients with AE. We found that these DEGs included genes closely related to tumor angiogenesis. This phenomenon should provide a molecular basis for AE invasion and help develop effective strategies for AE-targeted drug therapy.

METHODS

Patients and Samples

A total of 6 formalin-fixed paraffin-embedded (FFPE) surgical resection tissue samples, including 3 lesion samples as the experimental group (AE) and 3 surrounding liver parenchyma samples as the control group (AEC), from patients with AE with metastasis to the lymph nodes and distant organs, such as the lung, brain, spleen, diaphragm, gallbladder, kidney, and adrenal gland, were collected at the Department of Pathology of the First Affiliated Hospital of Xinjiang Medical University. The experimental group samples were limited to the area of host-parasite interface, as assessed based on observation of hematoxylin and eosin (H&E)-stained slides, excluding parasite components. For immunohistochemical analysis, 16 FFPE tissue samples from patients with metastatic AE, including 8 lesion samples and 8 surrounding liver parenchyma samples, were also collected at the Department of Pathology of the First Affiliated Hospital of Xinjiang Medical University. The samples had histopathological confirmation. Clinicopathological information was obtained from clinical records and pathology reports (the first 3 samples were also used for RNA sequencing analysis) (Table 1).

Ribonucleic Acid Quantification and Library Preparation

Total RNA was isolated using the TRIzol Reagent (Invitrogen, Carlsbad, CA), and RNA integrity was assessed using the RNA Nano 6000 Assay Kit of the Bioanalyzer 2100 system (Agilent Technologies, Santa Clara, CA). Sequencing libraries were generated [22] using the NEBNext UltraTM RNA Library Prep Kit for Illumina (NEB, Ipswich, MA) according to the manufacturer's recommendations. During the quality-control steps, real-time polymerase chain reaction (PCR) was performed using Phusion High-Fidelity DNA polymerase, universal PCR primers, and Index (X) Primer for the quantification and qualification of the sample library. Finally, the PCR products were purified using AMPure XP system (Beckman Coulter, Brea, CA) and library quality was assessed on an Agilent Bioanalyzer 2100 system.

Clustering and Sequencing

Clustering of the index-coded samples was performed on a cBot Cluster Generation System using a TruSeq PE Cluster Kit v3-cBot-HS (Illumina, San Diego, CA) according to the manufacturer's instructions. After cluster generation, the prepared libraries were sequenced on an Illumina Novaseq platform, and 150-base pair paired-end reads were generated. Raw data in the FASTQ format were first processed using Perl scripts developed in-house. In this step, clean data (clean reads) were obtained by removing reads containing adapters and poly-N, as well as low-quality reads, from the raw data. Concomitantly, the quality scores and GC content of the clean data were calculated. All downstream analyses were based on high-quality clean data.

Table 1. Demographic Characteristics and Clinical Data of Patients With AE

Number	Sex	Age	Location	PNM	Treatment Method
1	Female	40	Liver, lung, brain	P3N0M1	Autologous liver transplantation,
2	Male	52	Liver, kidney	P2N1M1	trefoil hepatectomy, unilateral nephrectomy, retroperitoneal tumor resection
3	Male	28	Liver, spleen	P2N1M1	staged spleen and left lateral lobe of liver resection
4	Male	50	Liver, brain, kidney, diaphragm	P4N1M1	Hemi-hepatectomy
5	Female	40	Liver, gallbladder	P3N1M0	Hemi-hepatectomy
6	Female	31	Liver, adrenal gland, lymph node	P2N1M0	Complex hepatic alveolar echinococcosis resection, adrenal alveolar echinococcosis resection
7	Male	62	Liver, gallbladder	P2N1M0	Hemi-hepatectomy, cholecystectomy
8	Male	29	Liver, lymph node	P2N1M0	Hemi-hepatectomy, regional lymphadenectomy

Abbreviations: AE, alveolar echinococcosis; PNM, polymorphonuclear.

Differential Expression Analysis

An index of the reference genome (Homo sapiens [GRch38/hg38], https://www.ncbi.nlm.nih.gov/grc/human/data?asm=GRCh38) was built, and paired-end clean reads were aligned to the reference genome using Hisat2 (v2.0.5) [23]. The mapped reads of each sample were assembled by StringTie (v1.3.3b) [24] using a reference-based approach. Subsequently, featureCounts (v1.5.0-p3) was used to count the number of reads mapped to each gene. The reads per kilobase transcriptome per million (RPKM) mapped reads method was used to normalize the gene expression levels [25]. The fragments per kilobase million (FPKM) of each gene was calculated based on its length and the read count was mapped to this gene. The differential expression analysis of 2 conditions or groups (2 biological replicates per condition) was performed using the DESeq2R package (1.20.0). The resulting P values were adjusted using the Benjamini-Hochberg method, to control the false discovery rate. Genes with |log 2(FoldChange)| >1 and $P < .05$, as assessed using DESeq2 (1.20.0), were assigned as being differentially expressed.

Enrichment Analysis of Differentially Expressed Genes

A Gene Ontology ([GO] http://www.geneontology.org/) enrichment analysis and a Kyoto Encyclopedia of Genes and Genomes ([KEGG] http://www.genome.jp/kegg/) pathway analysis of the DEGs were performed using the ClusterProfiler R package (3.4.4), in which the gene length bias was corrected. All DEGs were mapped to GO terms in the database, and GO terms with a corrected $P < .05$ were considered significantly enriched among the DEGs.

Tissue Microarray Construction and Immunohistochemical Staining

Representative areas of the FFPE tissue samples used for tissue microarray (TMA) construction were confirmed by H&E staining. Slides for each case were reviewed, and TMA was constructed using cores with a 2-mm diameter derived from selected areas from each tissue sample. The TMAs were sectioned at a thickness of 3 μm, and immunohistochemical staining of each slide, including positive and negative controls, was performed according to the manufacturer's instructions on Ventana Bench Mark Ultra (Roche, Tucson, AZ). The antibody markers used in this experiment included anti-CD34 (Zen-bio Inc., Research Triangle Park, NC), anti-VEGF (Proteintech, Chicago, IL), anti-ADAM12 (Affinity Biosciences, Cincinnati, OH), anti-APLN (Affinity Biosciences), anti-TWIST1 (Affinity Biosciences), anti-SPP1 (Affinity Biosciences), anti-RSPO3 (Affinity Biosciences), and anti-FOXC2 (Proteintech) antibodies. Scan files and images of immunohistochemical sections were collected using Pannoramic DESK (3D HISTECH, Budapest, Hungary) tissue-section digital scanner and imaging system and Pannoramic Scanner software. The Aipathwell digital pathological image analysis software (Servicebio, Wuhan, China) was used to automatically read the tissue measurement area, and the number of positive cells in the measurement area was analyzed and calculated, with 3 fields being analyzed and averaged for each slide. The histochemistry score (H-score) was used to grade the expression intensity of proteins based on the following equation: H-score = $\sum(pi \times i)$, in which i represents the intensity of staining, which was graded as 0 (no staining), 1 (weak), 2 (moderate), 3 (strong); and Pi represents the percentage of positive cells (0%–100%) [26].

Statistical Analysis

Data were analyzed using GraphPad Prism (version 5.03; GraphPad Software, Inc., San Diego, CA) and SPSS (version 22.0; SPSS, Inc., IBM Business Analytics, Armonk, NY). The parametric t test and Mann-Whitney test were used to analyze the immunohistochemical H-scores between groups. Statistical significance was set at $P < .05$.

Ethics Approval

All procedures were performed in adherence to the terms of the latest version of the Declaration of Helsinki for Medical Research involving Human Subjects and approved by the Ethical Committee of the First Affiliated Hospital of Xinjiang Medical University.

Patient Consent Statement

All included patients were provided with written informed consent for anonymous collection and analysis of clinical data.

RESULTS

Identification of Differentially Expressed Transcripts

A principal component analysis (PCA) of the RNA sequencing data was performed using the gene expression values (FPKM) of all samples in the experimental and control groups. The PCA plot identified the AE lesion samples from the adjacent parenchyma (Figure 1). A total of 99.4 and 111.1 million clean reads were obtained from AE lesion and surrounding liver parenchyma samples, respectively. Detailed information is provided in Table 2. A total of 1796 DEGs were found in the lesion specimens from patients with AE versus the paralesional specimens, of which 1742 genes were upregulated and 54 genes were downregulated, as shown in the volcano plot (Figure 2). The 10 most significantly upregulated and 10 most significantly downregulated genes are listed in Table 3. A heatmap highlighted the expression patterns of DEGs between the 2 sample groups (Supplementary Figure 1). We found that these DEGs included several genes related to epithelial-to-mesenchymal transition, tumor invasion, metastasis, and, especially, to tumor angiogenesis, such as *ADAM12*, *APLN*, *TWIST1*, *SPP1*, *RSPO3*, and *FOXC2*, as detailed in Table 4.

Functional Analysis of Differentially Expressed Genes

The GO functional enrichment analysis identified 206 GO terms that were significantly enriched for DEGs. With the exception of the top 30 most significantly enriched GO terms shown in

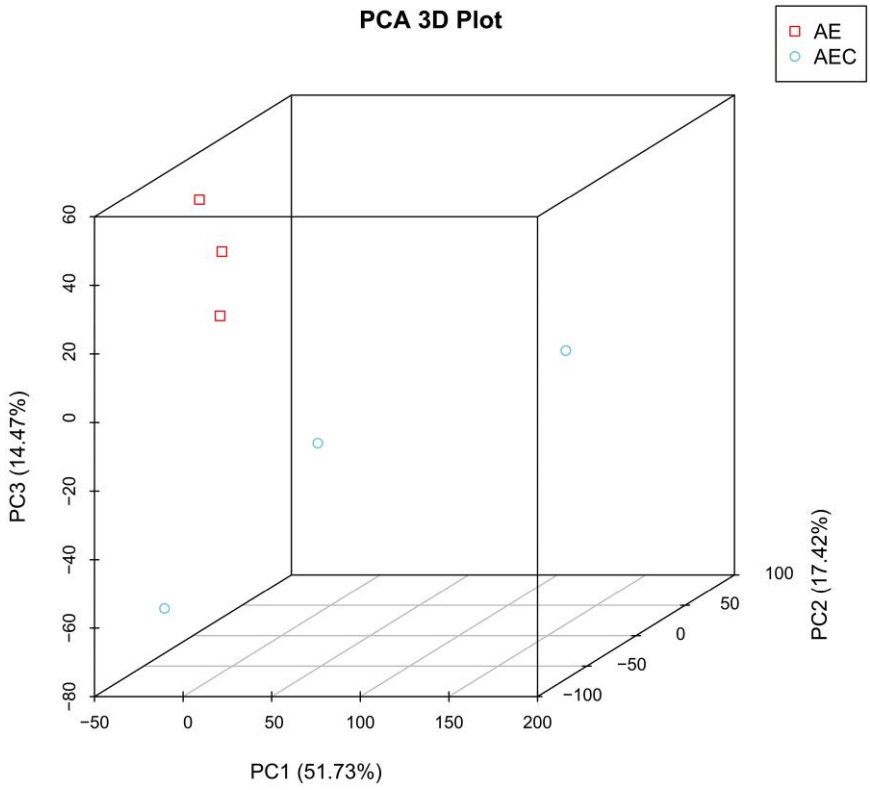

Figure 1. Principal component analysis (PCA) of the RNA sequencing data. A principal component analysis was performed on the gene expression values (FPKM) of all samples in the 2 groups. AE, alveolar echinococcosis; AEC, AE control group; PC1, first principal component; PC2, second principal component; PC3, third principal component.

Table 2. Alignment Statistics of Reads and Reference Genome (Homo Sapiens [GRch38/hg38])

Sample	Total Reads	Total Map	Unique Map	Multimap	Proper Map
AE1	34 909 784	27 543 036	24 187 962	3 355 074	23 182 746
		(78.9%)	(69.29%)	(9.61%)	(66.41%)
AE2	35 747 526	30 803 501	24 452 276	6 351 225	23 417 514
		(86.17%)	(68.4%)	(17.77%)	(65.51%)
AE3	28 723 542	26 227 080	24 850 277	1 376 803	23 725 442
		(91.31%)	(86.52%)	(4.79%)	(82.6%)
AEC1	31 481 438	26 474 178	23 458 011	3 016 167	22 688 640
		(84.09%)	(74.51%)	(9.58%)	(72.07%)
AEC2	36 255 914	10 881 113	9 322 237	1 558 876	9 003 862
		(30.01%)	(25.71%)	(4.3%)	(24.83%)
AEC3	43 405 302	29 554 703	28 616 703	938 000	27 836 652
		(68.09%)	(65.93%)	(2.16%)	(64.13%)

Abbreviations: AE, alveolar echinococcosis; AEC, AE control group.

Figure 3, there were terms related to tumor invasion and angiogenesis, such as sprouting angiogenesis (biological process [BP]), epithelial-to-mesenchymal transition (BP), and positive regulation of the ERK1 and ERK2 cascade (BP). The top 20 most significantly enriched pathways are reported in Figure 4. We also found that DEGs were enriched on pathways such as the Wnt signaling pathway, Hippo signaling pathway, and Hedgehog signaling pathway, which regulate cell proliferation, differentiation, and tumor metastasis. In addition, the enriched GO terms and KEGG pathways also included chemokine-mediated signaling pathway (BP), cytokine activity (molecular function [MF]), cytokine receptor binding (MF), and cytokine-cytokine receptor interaction (KEGG), which are related to the immune response, were also significantly enriched for DEGs.

Detection and Verification of Differentially Expressed Genes

The verification of the results of the transcriptome analysis was performed by immunohistochemical analysis of the

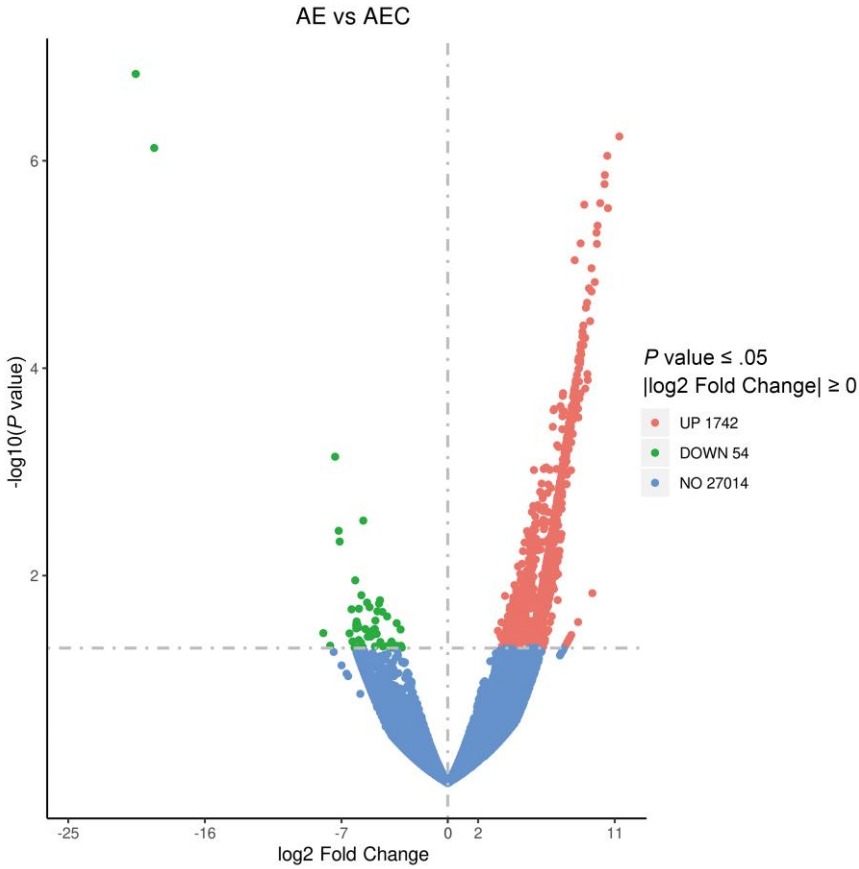

Figure 2. Volcano plot of the differentially expressed genes between the experimental (alveolar echinococcosis [AE]) and control (AE control group [AEC]) groups. The x-axis shows the differences in gene expression ($-\log_{10}$ *P* value), whereas the y-axis indicates expression changes (log2-fold change) of the genes in the different groups.

angiogenesis-related genes *ADAM12*, *APLN*, *TWIST1*, *SPP1*, *RSPO3*, and *FOXC2*. First, staining for CD34 in AE lesion samples showed different degrees of vascularization in the lesions, particularly at the host-parasite interface. Subsequently, the expression levels of selected genes were detected and analyzed. Upregulation of *ADAM12*, *APLN*, *TWIST1*, *SPP1*, *RSPO3*, and *FOXC2* was observed in the AE lesion samples, whereas low or no expression of these genes was detected in the paralesion samples. We also observed a positive expression of VEGF in AE lesion samples, especially in vascular ECs (Figure 5*A*). A quantitative analysis revealed that the levels of expression of *ADAM12*, *APLN*, *TWIST1*, *SPP1*, *RSPO3*, and *FOXC2* were significantly higher in the AE lesion samples compared with the paralesion samples ($P < .05$) (Figure 5*B*).

DISCUSSION

As a chronic infectious disease, AE is characterized by typical features of chronic inflammation, including an intense granulomatous structure surrounded by an extensive fibroinflammatory host reaction [21]. Conversely, the metacestode of *E multilocularis* tends to disseminate into organs other than the liver via local spreading or distant metastasis [27], thus hampering or precluding the treatment of AE. Therefore, to investigate the molecular mechanism involved in the aggressive, tumor-like biological behavior of AE, such as invasion and distant metastasis, and to provide a molecular basis for targeted drug therapy, we screened for DEGs in the samples of patients with AE with lymph node, lung, gallbladder, kidney, and brain invasion or metastasis using RNA-seq, and we verified the results using immunohistochemistry. First, several new blood vessels was observed in the AE lesion samples through CD34 immunohistochemical staining, particularly at the host-parasite interface, and VEGF expression was significantly upregulated. The RNA-sequence results showed that the DEGs in the AE lesions included a variety of genes involved in different biological processes and signaling pathways. Furthermore, as expected, we found that DEGs related to epithelial-to-mesenchymal transition, tumor invasion and metastasis, and especially tumor angiogenesis were significantly upregulated in the AE lesion group. As a specific characteristic of malignant tumors, angiogenesis plays an important role in the process of tumor

Table 3. Top 10 Up- or Downregulated DEGs in AE Lesion Samples

	Gene ID	Gene Name	Gene Description	Fold Change	*P* Value
Up	211935	*IGHV1-3*	immunoglobulin heavy variable 1–3	11.303	<.001
	172061	*LRRC15*	leucine rich repeat containing 15	10.508	<.001
	224729	*PCOLCE-AS1*	PCOLCE antisense RNA 1	10.347	<.001
	111012	*CYP27B1*	cytochrome P450 family 27 subfamily B member 1	10.329	<.001
	197506	*SLC28A3*	solute carrier family 28 member 3	10.042	<.001
	206384	*COL6A6*	collagen type VI alpha 6 chain	8.992	<.001
	211659	*IGLV3-25*	immunoglobulin lambda variable 3–25	10.549	<.001
	106976	*DNM1*	dynamin 1	9.867	<.001
	172752	*COL6A5*	collagen type VI alpha 5 chain	9.800	<.001
	198542	*ITGBL1*	integrin subunit beta like 1	8.752	<.001
Down	230258	*AC005208.1*	novel transcript	−20.553	<.001
	217408	*PRELID1P2*	PRELI domain containing 1 pseudogene 2	−20.553	<.001
	129514	*FOXA1*	forkhead box A1	−19.339	<.001
	081479	*LRP2*	LDL receptor-related protein 2	−7.420	<.001
	042832	*TG*	thyroglobulin	−5.564	.002
	177508	*IRX3*	iroquois homeobox 3	−7.186	.003
	069509	*FUNDC1*	FUN domain containing 1	−7.119	.004
	135114	*OASL*	2′−5′-oligoadenylate synthetase like	−6.095	.011
	228695	*CES1P1*	carboxylesterase 1 pseudogene 1	−5.691	.015
	138829	*FBN2*	fibrillin 2	−4.462	.017

Abbreviations: AE, alveolar echinococcosis; DEG, differentially expressed gene; ID, identification; LDL, low-density lipoprotein; RNA, ribonucleic acid.

Table 4. Angiogenesis Related DEGs in AE Lesion Samples

Gene ID	Gene Name	Gene Description	Fold Change	*P* Value
148848	*ADAM12*	mucosal vascular addressin cell adhesion molecule 1	6.183	.001
171388	*APLN*	apelin	6.928	.003
122691	*TWIST1*	twist family bHLH transcription factor 1	6.671	.005
118785	*SPP1*	secreted phosphoprotein 1	4.130	.023
146374	*RSPO3*	R-spondin 3	4.859	.023
176692	*FOXC2*	forkhead box C2	5.116	.029

Abbreviations: AE, alveolar echinococcosis; DEG, differentially expressed gene; ID, identification.

progression. Tumor cells develop an angiogenic phenotype that supports the further growth and distant metastasis of the tumor [28, 29]. The observation that highly vascularized tumors grow rapidly, whereas tumors with a low vessel density are rather dormant, led to the hypothesis that tumor angiogenesis is required for tumor progression [30]. Conversely, the vasculature of tumors can also result from an inflammatory reaction to necrotic tumor cells. Thus, the initial factor that triggers angiogenesis involves the action of an angiogenic stimulus, such as hypoxia or inflammation [31]. In this research, we found that GO terms and pathways related to the immune response, such as the chemokine-mediated signaling pathway, cytokine activity, cytokine receptor binding, and cytokine-cytokine receptor interaction, were also significantly enriched for DEGs. In the case of AE, the inflammation and fibrosis that occur during disease progression continue to damage liver cells and other tissues. Subsequently, necrosis may occur in the middle of the AE lesions, and necrotic substances further aggravate the inflammation. Accordingly, we can assume that the dissemination of the metacestode of *E multilocularis* may be maintained by continuous inflammation and tissue necrosis, and that new blood vessels at the host-parasite interface, in turn, facilitate the process of AE invasion and metastasis.

The DEGs detected in the AE lesion samples included *SPP1* (osteopontin), which encodes a glycoprotein that may be involved in cell attachment and signaling [32, 33]. SPP1 is closely involved in the regulation of the various factors that affect tumor progression, such as cellular proliferation, apoptosis, and metastasis, in several types of cancers [34, 35]. Previous studies have proved that, in ECs, SPP1 stimulates tumor angiogenesis by inducing VEGF secretion [36, 37]. R-spondin 3 (RSPO3), which is a member of a novel family of secreted proteins that activate Wnt/β-catenin signaling, plays a key role in embryonic vasculogenesis and tumor angiogenesis [38, 39] and promotes EC proliferation through VEGF signaling [40]. TWIST1, a basic helix-loop-helix domain-containing transcription factor, is an essential regulator of embryogenesis in many species. In humans, it has been shown to play an essential role in tumor progression, angiogenesis, invasion, and metastasis. TWIST1 promotes vascularization in tumor xenograft models [41, 42]. Overexpression of *TWIST1* is correlated with upregulation of VEGF and EC proliferation, and it induces angiogenesis in hepatocellular carcinoma [43] and breast cancer [41]. The well accepted metastasis-related gene *FOXC2* has been reported as an oncogene in a range of cancers. FOXC2 has been identified as a

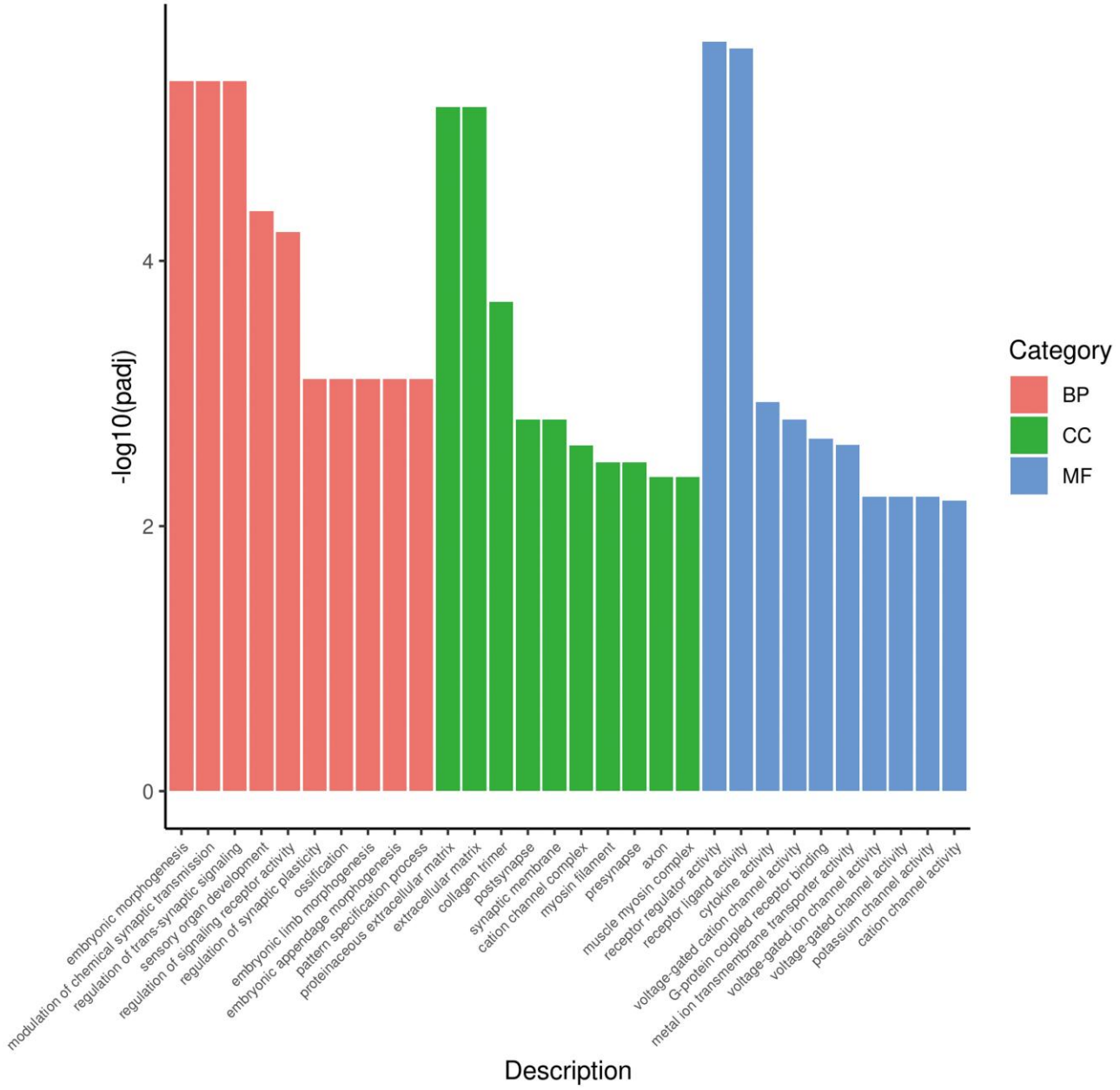

Figure 3. The top 30 most significantly enriched Gene Ontology (GO) terms between the experimental (alveolar echinococcosis [AE]) and control (AE control group [AEC]) groups. The y-axis label represents the significance level of enriched GO terms ($-\log_{10}$ *P* value), and the x-axis label represents the enriched GO terms. BP, biological process; CC, cellular component; MF, molecular function.

regulator of vascular formation and remodeling, thus controlling angiogenic processes by regulating the expression of vascular endothelial cell surface molecules, such as Ang-2 [44], CXCR4, and integrin-β3 [45, 46], which are involved in neovascularization. Recent research indicates that FOXC2 may facilitate the growth and invasion of HCC by regulating the proangiogenic protein Ang-2 [47]. The ADAMs family member *ADAM12*, which is a disintegrin and metalloprotease, has been reported to be markedly upregulated in a variety of human tumors [48]. In tumor cells, it may facilitate a proangiogenic tumor microenvironment that leads to enhanced tumor growth and metastasis [49]. *ADAM12* expression in breast tumor cells is correlated with a significant upregulation of proangiogenic factors, such as VEGF and MMP-9, with these *ADAM12*-mediated effects being driven by the activation of EGFR, STAT3, and Akt signaling [50]. APLN is one of the endogenous ligands of the G-protein-coupled receptor Apj, which is a potential surface marker of the tumor endothelium.

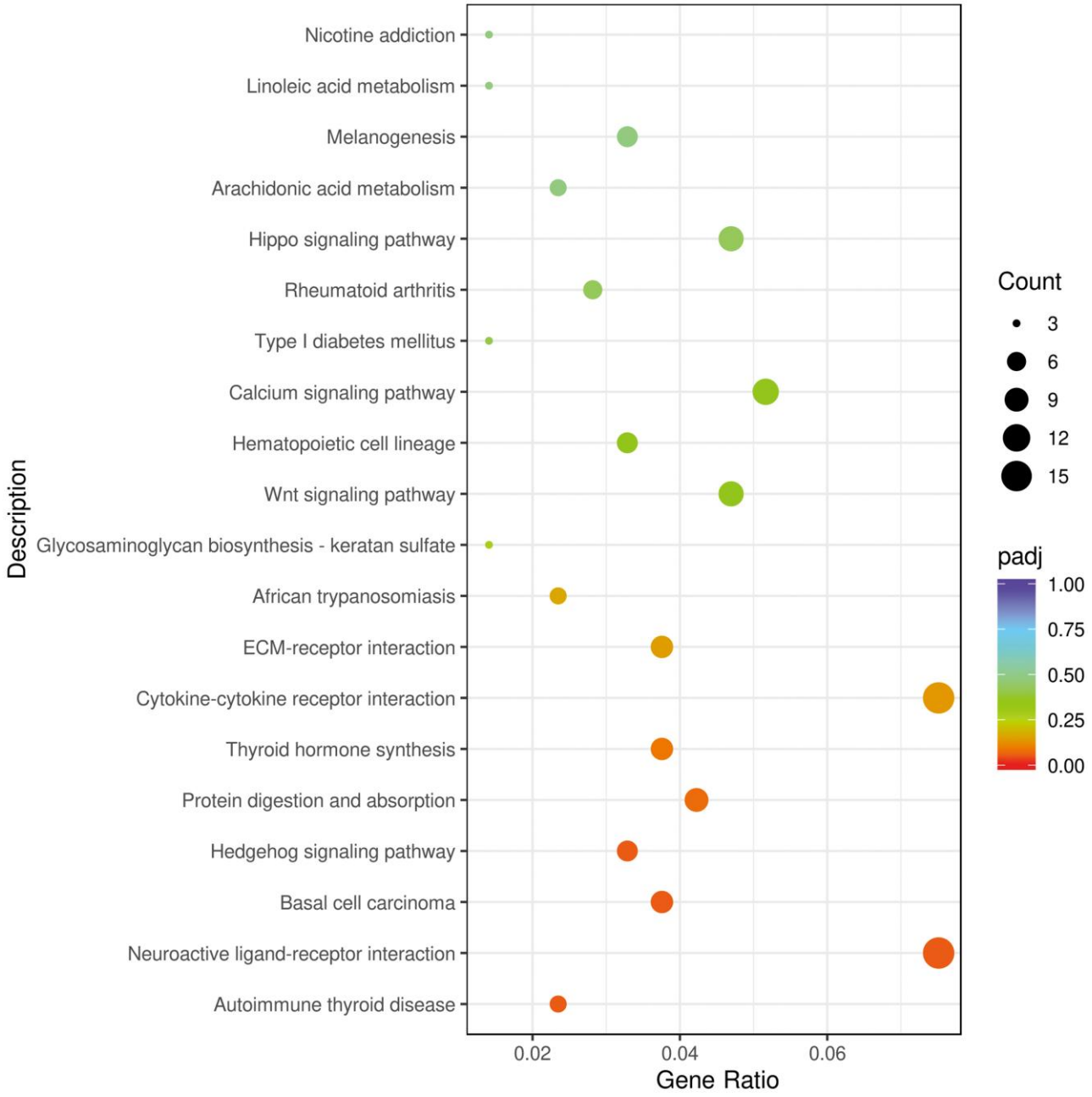

Figure 4. The top 20 most significantly enriched pathways between the experimental (AE) and control (AEC) groups. The y-axis label represents the distinct Kyoto Encyclopedia of Genes and Genomes (KEGG) pathways, and the x-axis label represents the gene ratio. The dot size is positively correlated with the number of differentially expressed genes. The colors of the dots represent the *P* values for the enrichment.

Previous studies have proven that *APLN* is enriched during neovascularization [51]. Moreover, it was recently reported that loss of *APLN* markedly reduced tumor angiogenesis, leading to impaired tumor growth in breast cancer and glioblastoma through VEGF and Noch signaling [52–54]. Based on these reports, and the results of our study, we can infer that the upregulation of these genes may contribute to the neovascularization that is commonly observed in the AE lesion samples, and that angiogenesis occurring during *E multilocularis* infection contributes strongly to the invasion and distant metastasis of AE.

CONCLUSIONS

In this study, we screened for gene expression signatures in the samples of patients with AE using transcriptome sequencing.

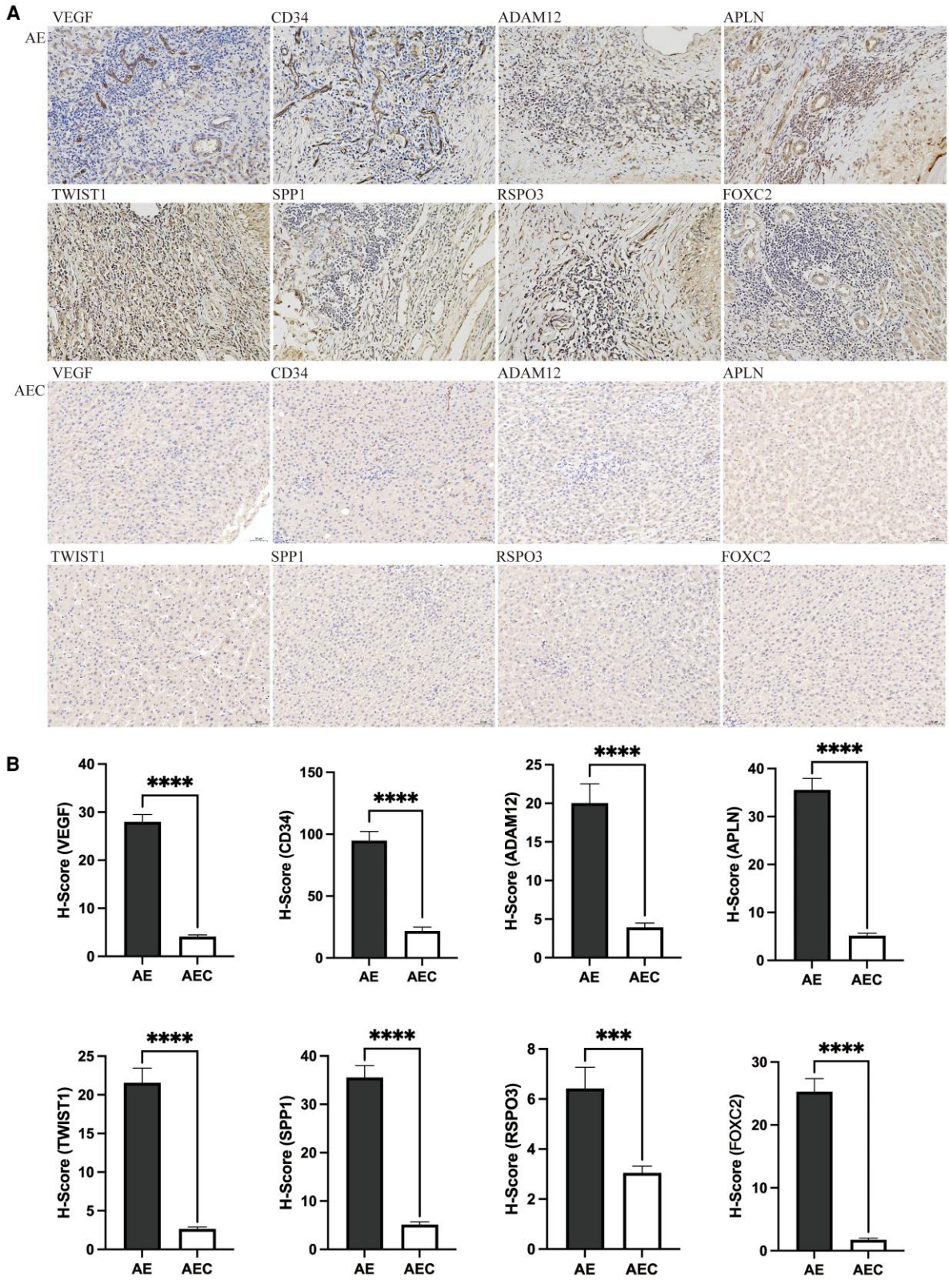

Figure 5. Immunohistochemical analysis of CD34, vascular endothelial growth factor (VEGF), and angiogenesis-related differentially expressed genes in the experimental (alveolar echinococcosis [AE]) and control (AE control group [AEC]) group samples. (*A*) CD34 and VEGF staining in AE samples showed different degrees of vascularization. Increased expression of *SPP1*, *RSPO3*, *APLN*, *TWIST1*, *ADAM12*, and *FOXC2* was observed in the AE samples, whereas low or no expression of these genes was observed in the AEC samples. (*B*) The *H*-scores of CD34, VEGF, SPP1, RSPO3, APLN, TWIST1, ADAM12, and FOXC2 were significantly higher in the AE samples than in the AEC samples (values represent the mean ± standard error of the mean: $***P < .001$, $****P < .0001$).

We found that these DEGs included several genes related to angiogenesis, which fit with our findings of vascularization and upregulated VEGF expression at the host-parasite interface, thus explaining the invasive and metastatic features of *E multilocularis* infection. These findings suggest new insights regarding the molecular mechanism of AE invasion and distant metastasis, and they provide new directions for targeted drug therapy.

Supplementary Data

Supplementary materials are available at *Open Forum Infectious Diseases* online. Consisting of data provided by the authors to benefit the reader, the posted materials are not copyedited and are the sole responsibility of the authors, so questions or comments should be addressed to the corresponding author.

Acknowledgments

Financial support. This work was supported by the Key Laboratory Open Research Program of State Key Laboratory on Pathogenesis, Prevention and Treatment of High Incidence Diseases in Central Asia (Grant No. SKL-HIDCA-2018-2).

Potential conflicts of interest. All authors: No reported conflicts of interest.

References

1. Deplazes P, Rinaldi L, Rojas C, et al. Global distribution of alveolar and cystic echinococcosis. Adv Parasitol **2017**; 95:315–93.
2. Mcmanus DP, Zhang W, Li J, Bartley PB. Echinococcosis. Lancet **2003**; 362: 1295–304.
3. Wen H, Dong JH, Zhang JH, et al. Ex vivo liver resection and autotransplantation for end-stage alveolar Echinococcosis: a case series. Am J Transplant **2016**; 16: 615–24.
4. Brunetti E, Kern P, Vuitton DA. Expert consensus for the diagnosis and treatment of cystic and alveolar echinococcosis in humans. Acta Trop **2010**; 114:1–16.
5. Piarroux M, Piarroux R, Giorgi R, et al. Clinical features and evolution of alveolar echinococcosis in France from 1982 to 2007: results of a survey in 387 patients. J Hepatol **2011**; 55:1025–33.
6. Craig P. Echinococcus multilocularis. Curr Opin Infect Dis **2003**; 16:437–44.
7. Deplazes P, Grimm F, Sydler T, Tanner I, Kapel CMO. Experimental alveolar echinococcosis in pigs, lesion development and serological follow up. Vet Parasitol **2005**; 130:213–22.
8. Eckert J, Deplazes P. Biological, epidemiological, and clinical aspects of echinococcosis, a zoonosis of increasing concern. Clin Microbiol Rev **2004**; 17:107–35.
9. Alessia P, Raúl M-R, Carlos S-O, et al. Potential risk factors associated with human cystic echinococcosis: systematic review and meta-analysis. PLoS Negl Trop Dis **2016**; 10:e0005114.
10. Carmeliet P. Angiogenesis in life, disease and medicine. Nature **2005**; 438:932–6.
11. Carmeliet P, Jain RK. Angiogenesis in cancer and other diseases. Nature **2000**; 407:249–57.
12. Ferrara N, Gerber HP, LeCouter J. The biology of VEGF and its receptors. Nat Med **2003**; 9:669–76.
13. Gerber HP, McMurtrey A, Kowalski J, et al. Vascular endothelial growth factor regulates endothelial cell survival through the phosphatidylinositol 3′-kinase/Akt signal transduction pathway. Requirement for Flk-1/KDR activation. J Biol Chem **1998**; 273:30336–43.
14. Ferrara N, Alitalo K. Clinical applications of angiogenic growth factors and their inhibitors. Nat Med **1999**; 5:1359–64.
15. Kerbel RS. Tumor angiogenesis. N Engl J Med **2008**; 358:2039–49.
16. Dennis RD, Schubert U, Bauer C. Angiogenesis and parasitic helminth-associated neovascularization. Parasitology **2011**; 138:426–39.
17. Stadelmann B, Spiliotis M, Müller J, et al. Echinococcus multilocularis phosphoglucose isomerase (EmPGI): a glycolytic enzyme involved in metacestode growth and parasite-host cell interactions. Int J Parasitol **2010**; 40:1563–74.
18. van Ginderachter JA, Beschin A, De Baetselier P, Raes G. Myeloid-derived suppressor cells in parasitic infections. Eur J Immunol **2010**; 40:2976–85.
19. Jian Hai Y, Yu Juan S, Ai Ping Y, Jian-Ping C. In vitro pro-angiogenic activity of Echinococcus granulosus hydatid cysts from experimentally infected mice. Zhongguo Xue Xi Chong Bing Fang Zhi Za Zhi **2017**; 29:20–323.
20. Pan W, Zhou HJ, Shen YJ, et al. Surveillance on the status of immune cells after Echinococcus granulosus protoscoleces infection in Balb/c mice. PLoS One **2013**; 8:e59746.
21. Vuitton DA, Gottstein B. Echinococcus multilocularis and its intermediate host: a model of parasite-host interplay. J Biomed Biotechnol **2010**; 2010:923193.
22. Parkhomchuk D, Borodina T, Amstislavskiy V, et al. Transcriptome analysis by strand-specific sequencing of complementary DNA. Nucleic Acids Res **2009**; 37:e123.
23. Mortazavi A, Williams BA, McCue K, Schaeffer L, Wold B. Mapping and quantifying mammalian transcriptomes by RNA-Seq. Nat Methods **2008**; 5:621–28.
24. Pertea M, Pertea GM, Antonescu CM, Chang T-C, Mendell JT, Salzberg SL. Stringtie enables improved reconstruction of a transcriptome from RNA-seq reads. Nat Biotechnol **2015**; 33:290–95.
25. Bray NL, Pimentel H, Melsted P, Pachter L. Near-optimal probabilistic RNA-Seq quantification. Nat Biotechnol **2016**; 34:525–7.
26. Dogan S, Vasudevaraja V, Xu B, et al. DNA methylation-based classification of sinonasal undifferentiated carcinoma. Mod Pathol **2019**; 32:1447–59.
27. Moro P, Schantz PM. Echinococcosis: a review. Int J Infect Dis **2009**; 13:125–33.
28. Loizzi V, del Vecchio V, Gargano G, et al. Biological pathways involved in tumor angiogenesis and bevacizumab based anti-angiogenic therapy with special references to ovarian cancer. Int J Mol Sci **2017**; 18:1967.
29. Li T, Kang G, Wang T, Huang H. Tumor angiogenesis and anti-angiogenic gene therapy for cancer. Oncol Lett **2018**; 16:687–702.
30. Folkman J. Angiogenesis in cancer, vascular, rheumatoid and other disease. Nat Med **1995**; 1:27–31.
31. Duran CL, Howell DW, Dave JM, et al. Molecular regulation of sprouting angiogenesis. Compr Physiol **2017**; 8:153–235.
32. Mohammadi S, Ghaffari SH, Shaiegan M, et al. Curcumin veto the effects of osteopontin (OPN) specific inhibitor on leukemic stem cell colony forming potential via promotion of OPN overexpression. Int J Hematol Oncol Stem Cell Res **2016**; 10:120–9.
33. Mohammadi S, Ghaffari SH, Shaiegan M, et al. Acquired expression of osteopontin selectively promotes enrichment of leukemia stem cells through AKT/mTOR/PTEN/beta-catenin pathways in AML cells. Life Sci **2016**; 152:190–8.
34. Lin J, Myers AL, Wang Z, et al. Osteopontin (OPN/SPP1) isoforms collectively enhance tumor cell invasion and dissemination in esophageal adenocarcinoma. Oncotarget **2015**; 6:22239–57.
35. Weber GF. The cancer biomarker osteopontin: combination with other markers. Cancer Genomics Proteomics **2011**; 8:263–88.
36. Senger DR, Ledbetter SR, Claffey KP, Papadopoulos-Sergiou A, Peruzzi CA, Detmar M. Stimulation of endothelial cell migration by vascular permeability factor/vascular endothelial growth factor through cooperative mechanisms involving the alphavbeta3 integrin, osteopontin, and thrombin. Am J Pathol **1996**; 149:293–305.
37. Chakraborty G, Jain S, Kundu GC. Osteopontin promotes vascular endothelial growth factor-dependent breast tumor growth and angiogenesis via autocrine and paracrine mechanisms. Cancer Res **2008**; 68:152–61.
38. Nam JS, Turcotte TJ, Smith PF, Choi S, Yoon JK. Mouse cristin/R-spondin family proteins are novel ligands for the Frizzled 8 and LRP6 receptors and activate beta-catenin-dependent gene expression. J Biol Chem **2006**; 281:13247–57.
39. Kim KA, Wagle M, Tran K, et al. R-spondin family members regulate the Wnt pathway by a common mechanism. Mol Biol Cell **2008**; 19:2588–96.
40. Kazanskaya O, Ohkawara B, Heroult M, et al. The Wnt signaling regulator R-spondin 3 promotes angioblast and vascular development. Development **2008**; 135:3655–64.
41. Mironchik Y, Winnard PT Jr, Vesuna F, et al. Twist overexpression induces in vivo angiogenesis and correlates with chromosomal instability in breast cancer. Cancer Res **2005**; 65:10801–9.
42. Tseng JC, Chen HF, Wu KJ. A twist tale of cancer metastasis and tumor angiogenesis. Histol Histopathol **2015**; 30:1283–94.
43. Niu RF, Zhang L, Xi GM, et al. Up-regulation of twist induces angiogenesis and correlates with metastasis in hepatocellular carcinoma. J Exp Clin Cancer Res **2007**; 26:385–94.
44. Xue Y, Cao R, Nilsson D, et al. FOXC2 controls Ang-2 expression and modulates angiogenesis, vascular patterning, remodeling, and functions in adipose tissue. Proc Natl Acad Sci U S A **2008**; 105:10167–72.
45. Hayashi H, Kume T. Forkhead transcription factors regulate expression of the chemokine receptor CXCR4 in endothelial cells and CXCL12-induced cell migration. Biochem Biophys Res Commun **2008**; 367:584–9.
46. Hayashi H, Sano H, Seo S, Kume T. The Foxc2 transcription factor regulates angiogenesis via induction of integrin beta3 expression. J Biol Chem **2008**; 283: 23791–800.
47. Chen J, Rong X, Liu X, et al. FOXC2 Is a prognostic biomarker and contributes to the growth and invasion of human hepatocellular carcinoma. Cancer Cell Int **2020**; 20:196.

48. Thodeti CK, Frohlich C, Nielsen CK, et al. Hierarchy of ADAM12 binding to integrins in tumor cells. Exp Cell Res **2005**; 309:438–50.
49. Le Pabic H, Bonnier D, Wewer UM, et al. ADAM12 In human liver cancers: TGF-beta-regulated expression in stellate cells is associated with matrix remodeling. Hepatology **2003**; 37:1056–66.
50. Roy R, Dagher A, Butterfield C, Moses MA. ADAM12 is a novel regulator of tumor angiogenesis via STAT3 signaling. Mol Cancer Res **2017**; 15:1608–22.
51. Yang P, Read C, Kuc RE, et al. Elabela/toddler is an endogenous agonist of the apelin APJ receptor in the adult cardiovascular system, and exogenous administration of the peptide compensates for the downregulation of its expression in pulmonary arterial hypertension. Circulation **2017**; 135:1160–73.
52. Mastrella G, Hou M, Li M, et al. Targeting APLN/APLNR improves antiangiogenic efficiency and blunts proinvasive side effects of VEGFA/VEGFR2 blockade in glioblastoma. Cancer Res **2019**; 79:2298–313.
53. Uribesalgo I, Hoffmann D, Zhang Y, et al. Apelin inhibition prevents resistance and metastasis associated with anti-angiogenic therapy. EMBO Mol Med **2019**; 11:e9266.
54. Frisch A, Kalin S, Monk R, et al. Apelin controls angiogenesis-dependent glioblastoma growth. Int J Mol Sci **2020**; 21:4179.